Mean-field predictions for a dipolar Bose-Einstein condensate with ^{164}Dy

Damir Zajec[1,*] and Günter Wunner[1]

[1] *Institut für Theoretische Physik 1, Universität Stuttgart, 70550 Stuttgart, Germany*

(Dated: October 22, 2015)

Dipolar Bose-Einstein condensates are systems well-suited for the investigation of effects caused by the non-local and anisotropic dipole-dipole interaction. In this paper we are interested in properties which are directly connected to the realization of a condensate with ^{164}Dy, such as stability and phase diagrams. Additionaly, we study the expansion of dipolar condensates, and find signatures of the dipole-dipole interaction in terms of structured states and a deviation of the well-known inversion of the aspect ratio of the cloud during a time of flight. Our analysis is based on the extended Gross-Pitaevskii equation, which we solve numerically exact on a grid by means of an imaginary- and real-time evolution.

PACS numbers: 05.45.-a, 67.85.-d, 74.50.+r

I. INTRODUCTION

The realization of dipolar Bose-Einstein condensates (BECs) with large magnetic moments is an important step towards the opportunity for a more detailed study of the effects caused by the nonlinear, anisotropic, non-local, and long-ranged dipole-dipole interaction (DDI), such as structured ground states [1, 2], solitons [3–6], and roton-maxon spectra [7]. Dipolar condensates have recently been realized with atoms of ^{52}Cr [8–10], ^{164}Dy [11, 12] and ^{168}Er [13]. Furthermore, there has been vast progress in the realization of a condensate with polar molecules with an electric dipole moment [14].

Two examples for the recent study of effects due to the DDI have been the experimental investigation of the collapse dynamics [15] and the inversion of the aspect ratio of the cloud [16] of a dipolar ^{52}Cr BEC. In the former case the scattering length was ramped down below the collapse threshold and absorption images were made after the collapse and explosion of the condensate. The density distribution inherited the d-wave symmetry $1-3\cos^2\vartheta$ of the DDI. In the latter case the dipolar forces were shown to inhibit the inversion of the aspect ratio of the cloud, which usually occurs during a time of flight. An exhaustive review of the physics of dipolar quantum gases has recently been given by Lahaye *et al.* [10] and Baranov *et al.* [17].

In this paper, we use the extended Gross-Pitaevskii equation to calculate the dynamics of a condensate, which yields an accurate describtion for sufficiently low temperatures and reads

$$\begin{aligned} H\psi(\boldsymbol{r},t) &= \left(-\frac{1}{2}\Delta + V_{\mathrm{har}} + V_{\mathrm{dd}} + V_{\mathrm{sc}}\right)\psi(\boldsymbol{r},t) \\ &= \mathrm{i}\partial_t\psi(\boldsymbol{r},t)\,, \end{aligned} \tag{1}$$

with

$$\begin{aligned} V_{\mathrm{har}} &= \frac{1}{2}(\omega_x^2x^2+\omega_y^2y^2+\omega_z^2z^2)\,, \\ V_{\mathrm{dd}} &= 3Na_{\mathrm{dd}}\int \mathrm{d}^3r'\frac{1-3\cos^2\vartheta}{|\boldsymbol{r}-\boldsymbol{r}'|^3}|\psi(\boldsymbol{r}',t)|^2\,, \\ V_{\mathrm{sc}} &= 4\pi Na|\psi(\boldsymbol{r},t)|^2\,. \end{aligned}$$

Here N is the number of particles, a_{dd} is the dipole length, and a denotes the scattering length. The dipoles are aligned along the z-axis, such that ϑ is the angle between the z-axis and the vector $\boldsymbol{r}-\boldsymbol{r}'$. This form implies that all lengths are scaled in units of $\sqrt{\hbar/m}$ and all energies in units of $\hbar$. The quantities Na and Na_{dd} control the strength of the scattering and the dipole interaction, respectively, and are assumed to be independently adjustable. The ratio $\epsilon = a_{\mathrm{dd}}/a$ is a measure for the importance of the dipole interaction. The strength of short-ranged interactions, which can be described by a Fermi-like contact interaction, can be controlled by means of a Feshbach-resonance [18, 19]. An external magnetic field changes the coupling between a bound state and a state of an incoming particle and allows for the control of the scattering length. This can be used to increase ϵ and therefore to enhance the dipolar character of the condensate. However, since Feshbach-resonances reduce the lifetime of a condensate, one prefers the realization of condensates with larger magnetic moments. Of all the above mentioned species with permanent magnetic dipole moments, ^{164}Dy stands out with $\mu = 10\mu_{\mathrm{B}}$, where μ_{B} is the Bohr magneton.

Our results can be scaled and are therefore valid for all dipolar systems. However, we are in particular interested in a condensate with ^{164}Dy, which means that in the following all parameters are adjusted to fit the needs of a condensate with this species. To the best of our knowledge, this is the first fully numerical three-dimensional study for a realistic set of parameters close to those in actual experimental setups. We emphasize that our calculations do not depend on any further simplifications or restrictions beyond the use of a mean-field ansatz.

In the next section we give a short introduction to our

* zajec@itp1.uni-stuttgart.de

numerical method and present our results with respect to expansion dynamics, structured ground states and a self-induced Josephson junction.

II. CONDENSATE WAVE FUNCTIONS

We solve the Gross-Pitaevskii equation numerically exact on a grid by means of the split-operator method using the imaginary- and real-time evolution. This yields a series of Fourier transforms, which we evaluate with a highly parallelized algorithm using the CUDA-architecture of NVIDIA. A more detailed overview is given in [6]. For the calculation of stability and phase diagrams we start with a simple Gaussian for a set of parameters far away from the stability border. This border is given by the maximum value (in this paper either the angle of rotation α or the number of particles N) for which the imaginary-time evolution converges and a stationary ground state exists. After the calculation of the ground state, we use this wave function as the initial wave function for the calculation of the next set of parameters, where we keep the aspect ratio or ϵ constant until we reach the stability border. Since our computational ressources allow for a very small step size, we can make very precise predictions with respect to stability and phase diagrams.

A. Expansion dynamics

One possible setup for the experimental investigation of dipolar signatures in condensates is to tilt the polarization axis with respect to the external confinement by means of an external magnetic field and investigate its expansion dynamics. The influence of the DDI should manifest itself in a deviation of the expansion dynamics as compared to a condensate which is strongly dominated by isotropic short-ranged interactions. The most clear evidence would be a TOF (time of flight) sequence in which the direction of the largest width of the cloud coincides with the polarization axis, regardless of the initial confinement. In this paper we study the equivalent scenario, where we rotate the external trap and the dipoles remain permanently aligned in z-direction. A tilt of the polarization axis clockwise in the xz-plane corresponds to a rotation of the trap anti-clockwise along the y-direction. The corresponding transformation of the coordinates reads

$$\begin{aligned} x' &= x\,\cos\,\alpha + z\,\sin\,\alpha, \\ y' &= y, \\ z' &= -x\,\sin\,\alpha + z\,\cos\,\alpha. \end{aligned} \tag{2}$$

Fig. 1 shows absorption images of three TOF sequences with $\epsilon = 1.1$ and different rotation angles α. For absorption images in the y- and z-direction we integrate $|\psi|^2$ along the y- and z-axis, respectively. The first seqence at the top shows a TOF for initial harmonic trapping with $\omega_{x,y,z} = 2\pi\cdot(205, 195, 760)$ Hz and $\alpha = 60°$, where we have used the trapping parameters from [12]. Since an anisotropic confinement yields an anisotropic momentum distribution, we see an inversion of the aspect ratio of the cloud. The TOF does not show any signature of the dipole-dipole interaction since the dynamics of the condensate is dominated almost entirely by the anisotropic momentum distribution. Therefore in the middle panels we reduce the aspect ratio of the trap and adjust the confinement to $\omega_{x,y,z} = 2\pi\cdot(205, 195, 360)$ Hz and $\alpha = 45°$. For this setup the dynamics of the condensate is in stark contrast to the TOF above since the expansion seems to be governed by the direction of the strongest initial confinement and the polarization axis. This can be cleary seen by the fact, that the direction of smallest width for

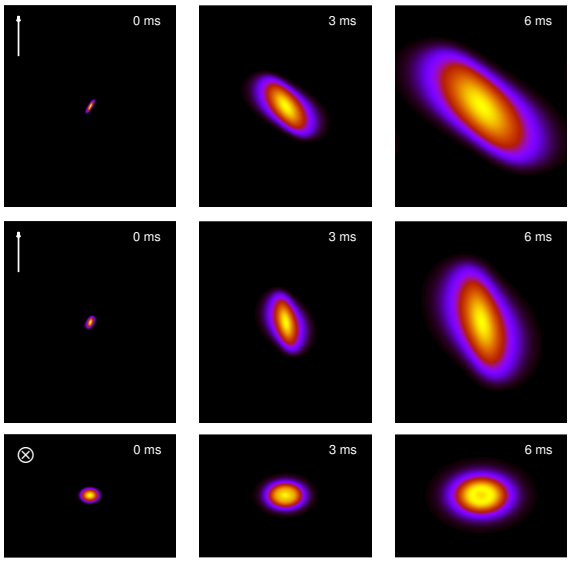

FIG. 1. (Color online) Absorption images in y- and z-direction ($|\psi|^2$ integrated along the y- and z-axis, respectively) for three different expansions of the condensate at times $t = 0, 3$ and 6 ms (from left to right). The symbol in the left top corner illustrates the polarization axis, which always points into the z-direction. Top: Absorption images in y-direction (x abscissa, z ordinate) $\perp$ polarization axis with $\omega_{x,y,z} = 2\pi\cdot(205, 195, 760)$ Hz, $\epsilon = 1.1$ and $\alpha = 60°$. The expansion is dominated by the anisotropy of the momentum distribution. Center: Absorption images in y-direction (x abscissa, z ordinate) $\perp$ polarization axis with $\omega_{x,y,z} = 2\pi\cdot(205, 195, 360)$ Hz, $\epsilon = 1.1$ and $\alpha = 45°$. Here the anisotropy in the momentum distribution is lower than in the upper case, which yields an expansion dynamics showing a clear signature of the dipole-dipole interaction. Bottom: Absorption images in z-direction (x abscissa, y ordinate) $\parallel$ polarization axis with $\omega_{x,y,z} = 2\pi\cdot(205, 195, 760)$ Hz, $\epsilon = 1.1$ and $\alpha = 0°$. Here the occurence of structured states during the TOF is recognizable (see also Fig. 2).

0 ms is not the direction which dominates the TOF, as is the case for the sequence above. Therefore this expansion dynamics strikes a balance between the direction that is given by the anisotropic momentum distribution and the polarization direction which is energetically preferable. The last TOF shows absorption images in z-direction for $\omega_{x,y,z} = 2\pi \cdot (205, 195, 760)$ Hz and $\alpha = 0°$. Here we see a blood-cell structured condensate where the density peak is away from the center [2], which occurs about 6 ms after the release from the trap (for better visibility see Fig. 2). Note that the initial density distribution in the xy-plane is given by a Gaussian. Therefore the structured state is not an artifact from the stationary ground state but rather a product of the expansion dynamics.

The crucial parameter for the experimental oberservation of structured states is the visibility

$$c = \frac{n_{\max} - n_{\min}}{n_{\max} + n_{\min}}, \tag{3}$$

where

$$n = \int \mathrm{d}z |\psi(\boldsymbol{r})|^2, \tag{4}$$

with $n_{\max}$ as the maximum value and $n_{\min}$ as the value in the center of the plane. The visibility c should be at least at about 0.1 to allow for a high-contrast imaging of the density distribution. It turns out that for all angles α the visibility is smaller than this benchmark. For the smallest angle $\alpha = 0°$ we find $c = 0.023$, whereas for $\alpha = 30°$ the corresponding visibility is $c = 0.006$. Additionaly, as can be seen in Fig. 2, where we depict the quantities

$$\begin{aligned} |\Psi_x|^2 &= \int \mathrm{d}z |\psi(x, 0, z)|^2 \\ |\Psi_y|^2 &= \int \mathrm{d}z |\psi(0, y, z)|^2, \end{aligned} \tag{5}$$

the rotation of the external confinement destroys the rotational symmetry in the xy-plane and leads to a saddle-shaped structured state.

The small value of c during the expansion dynamics suggests that such structured states can only be seen if modern imaging systems are further improved or systems with very large dipolar moments such as polar molecules are used.

B. Structured ground states

Structured states are not only a feature of dynamical processes, but do occur as stationary ground states as well. In this section we investigate where in the parameter space these structured states occur and if their visibility is large enough to satisfy the above mentioned criterion of $c \gtrsim 0.1$. Fig. 3 depicts the stability border

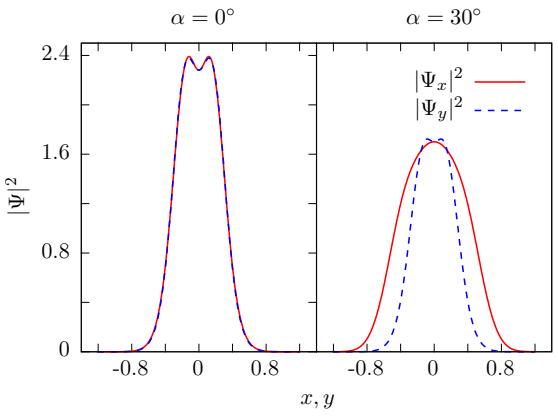

FIG. 2. (Color online) One-dimensional absorption images in z-direction for $\alpha = 0°$ and $\alpha = 30°$ after 6 ms of TOF. Note that for $\alpha = 0°$, the graphs for the quantities $|\Psi_x|^2$ and $|\Psi_y|^2$ are congruent. Since the visibility c of the structures decreases with an increase of α the largest value of $c = 0.023$ is given for $\alpha = 0°$. This is below the benchmark of $c \approx 0.1$, which is a necessary condition for the experimental observation of such structures. Additionaly, we see that the rotation of the trap destroys the rotational symmetry in the xy-plane.

for four different values of ϵ and a phase diagram of the visibility of structured ground states for $\epsilon = 1.3$ with respect to the angle of rotation α and the aspect ratio of the trap $\lambda = \omega_z/\omega_{x,y}$ with $\omega_z = 2\pi \cdot 760$ Hz, and $Na_{\mathrm{dd}} = 3.6$, which corresponds to 10^4 particles. An increase of the angle of rotation or a reduction of the aspect ratio results in more dipoles in the attractive head-to-tail configuration, and thus destabilizes the condensate. These parameters are therefore crucial for the stability properties of a dipolar condensate and can be used to investigate its stability borders.

Experimentally one would prefer to change the axis of polarization as opposed to the aspect ratio of the trap since this axis can be easily controlled by an external magnetic field. As one would expect, smaller values of ϵ, which correspond to a condensate less dominated by the DDI, stabilize the condensate against larger angles of rotation and smaller aspect ratios.

Structured states can be found in the vicinity of the border of stability. Here we find a broad strip in which $c \approx 0.1$. For low values of α, these structures resemble the blood-cell-like structured condensates (in the plane $\perp$ polarization axis) which also occur during the TOF (see Fig. 1). The spatial size of the structures is limited by the external confinement. Here the diameter of the ring $\gtrsim 1$ μm. This should be sufficient for an experimental observation.

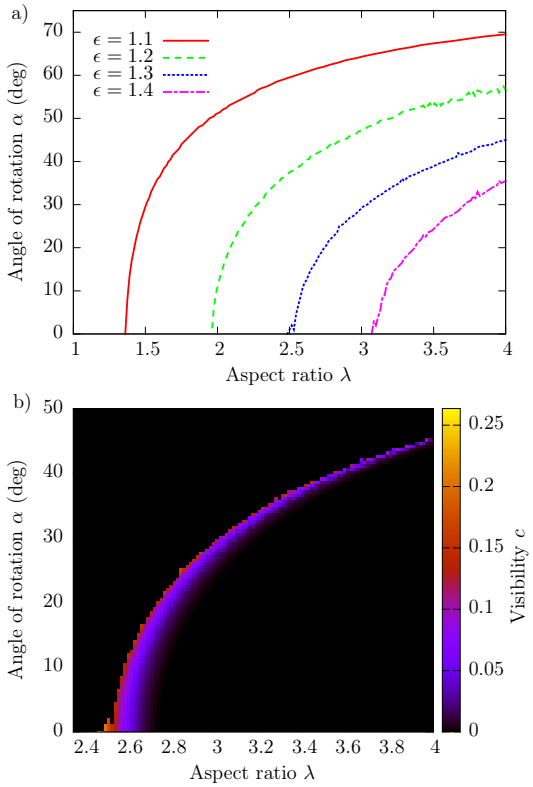

FIG. 3. (Color online) a) Stability diagrams for four values of ϵ with respect to the angle of rotation α and the aspect ratio of the trap $\lambda = \omega_z/\omega_{x,y}$ with $\omega_z = 2\pi \cdot 760$ Hz, and $Na_{\mathrm{dd}} = 3.6$ (which corresponds to 10^4 particles). We have plotted the maximum value of α which allows for a stable condensate for a given aspect ratio λ. A smaller value of ϵ stabilizes the condensate against the unstable head-to-tail configuration, which corresponds to large angles of rotation and small aspect ratios. b) Phase diagram for the visibility c for $\epsilon = 1.3$. Structured stationary ground states appear at the border of stability. Since we find $c \approx 0.1$ for a broad strip, an experimental observation should be possible.

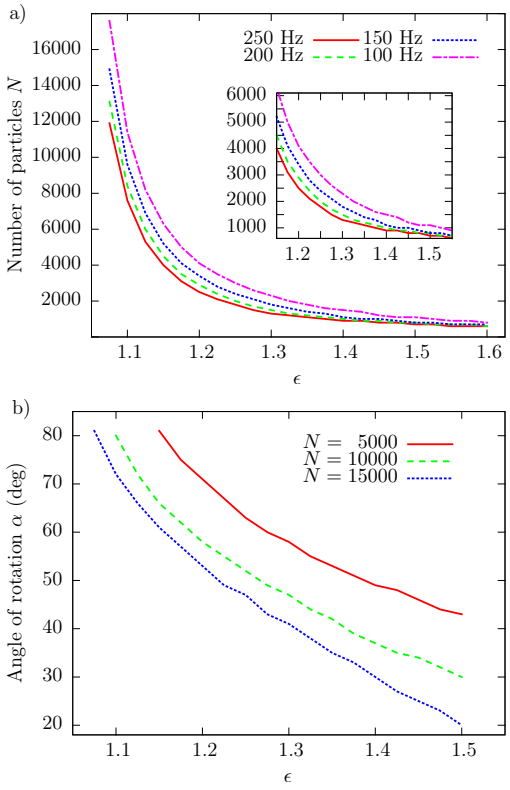

FIG. 4. (Color online) a) Stability diagram with respect to the number of particles N and ϵ. Here we have chosen $\alpha = 90°$, $\omega_{x,y} = 2\pi \cdot 50$ Hz and four different values of ω_z, where we have plotted the maximum value of N for a given ratio ϵ which allows for a stable condensate. An increase of N or ϵ destabilizes the condensate due to the DDI. b) Stability diagram with respect to the angle of rotation α and ϵ for $\omega_{x,y,z} = 2\pi \cdot (50, 50, 250)$ Hz and three different values for N, where we have plotted the maximum admissible value of α. Reducing α stabilizes the condensate und therefore allows for a greater amount of particles in the condensates.

C. Self-induced Josephson junction

One fascinating feature of dipolar condensates is the possibility of a self-induced Josephson junction, where the effective potential consisting of the external confinement and the dipolar potential has the form of a double well. These systems show well known phenomena such as Josephson oscillations or running phase modes [20]. In this subsection we are again interested in stability borders, now with respect to the number of particles N, the angle of rotation α, and ϵ. The self-induced Josephson junction can be realized by adding a toroidal potential to the external confinement. The external potential then reads

$$V_{\mathrm{ext}} = \frac{1}{2}(\omega_x^2 x^2 + \omega_y^2 y^2 + \omega_z^2 z^2) + V_0 e^{-2(x^2+y^2)/\sigma_0^2}, \quad (6)$$

with $V_0 = 3.286 \cdot 10^5$ (2.5 μK) and $\sigma_0 = 0.0764$ (5 μm). For $\alpha = 0°$ the Gaussian potential is in the xy-plane and therefore perpendicular to the axis of polarization. This is the most stable configuration of the torodial confinement since most of the dipoles are in the repulsive side-by-side configuration and arranged in a circle. If we rotate the trap until we attain $\alpha = 90°$, the axis of polarization and the Gaussian potential will be in the same plane and we obtain the anisotropic density distribution which corresponds to a double-well potential.

Fig. 4 depicts the stability diagrams with respect to

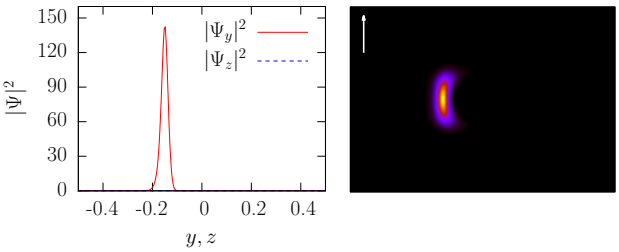

FIG. 5. (Color online) One- and two-dimensional absorption image in x-direction (y abscissa, z ordinate) $\perp$ polarization axis with $\alpha = 90^\circ$, $\omega_{x,y,z} = 2\pi \cdot (50, 50, 250)$ Hz, $\epsilon = 1.5$, and $N = 700$. The symbol in the left top corner illustrates the polarization axis, which points into the z-direction. The density distribution has the structure of a macroscopic quantum-self trapping state.

the number of particles N and ϵ as well as the angle of rotation α and ϵ. For the first diagram we have chosen $\alpha = 90^\circ$ and $\omega_{x,y} = 2\pi \cdot 50$ Hz and depict the stability diagram for four different values of ω_z. As can be seen, self-induced Josephson junctions cannot be realized with large numbers of ^{164}Dy particles. But it is possible to increase the number of particles by reducing the harmonic confinement ω_z. This leads to more dipoles in the repulsive side-by-side configuration and thus stabilizes the condensate. A more effective way of stabilizing the condensate is to choose a smaller angle of rotation. For the stability diagram with respect to α and ϵ we have chosen three different values for the number of particles and $\omega_{x,y,z} = 2\pi \cdot (50, 50, 250)$ Hz. We see again that reducing the number of particles stabilizes the condensate, and also that the reduction of α allows for a greater amount of particles in the condensate.

The calculation of stability diagrams allows for the search of new quantum states along the stability border of the self-induced Josephson junction. Indeed, we find a new stationary state whose density distribution corresponds to the macroscopic quantum self-trapping (MQST) state known from double-well potentials [21], in which only one well is occupied. We find this state in a small strip along the stability border in Fig. 4 a) for $\epsilon \gtrsim 1.325$. Fig. 5 depicts the one- and two-dimensional absorption images in x-direction of this state, where $|\Psi_{y,z}|^2$ is calculated analogously to (5). This state is robust with respect to small experimental imperfections like small perturbations in the horizontality of the toroidal trap. Indeed, the whole trap, as well as exclusively, the toroidal trap, may be rotated by several degrees without destroying this MQST-like state. Further imperfections like gradients in the magnetic field may affect in which well the particles of the condensate accumulate, but we do not expect any further consequences due to the small magnitude of the gradient (usually ≈ 1 Gauss/cm). Nonetheless, the effect of small gradients upon the accumulation of the particles can be investigated by aligning the dipoles parallel to the y-axis. Note that disturbances in general can result in a shift of the stability diagram, thus slightly changing the parameters where structured states are expected to appear.

Signatures of this MQST-like state can also be observed in the dynamics of Josephson junctions, where a large initial imbalance in the occupation of the wells cannot be periodically compensated and is therefore dominated by the self trapping in one well. This results in a running phase mode, where the creation of vortex-antivortex pairs in regions of small density is responsible for a phase shift [22].

III. CONCLUSION

We have presented a series of stability and phase diagrams with respect to parameters which are of great importance for the experimental investigation of a dipolar BEC. Our results are valid for all dipolar systems, but we have adjusted all parameters to fit the needs of a condensate with ^{164}Dy. We studied the expansion dynamics of a dipolar condensate and found two sorts of dipolar signatures occuring during TOF sequences: The effects of the DDI are noticeable in that the width of the spatially expanding cloud is not only governed by the anisotropic momentum distribution but also by the direction of the polarization axis. In addition, structured states occur during the TOF. The analysis of stability diagrams shows that structured ground states can be found along the stability border and that their visibility is large enough for modern imaging systems. We have shown that the realization of a self-induced Josephson junction with ^{164}Dy is restricted to a rather small amount of particles. However, this can be compensated by a rotation of the external confinement or the polarization axis. Finally, the analysis of the stability diagram shows that large values of ϵ allow for a macroscopic quantum self-trapping state. Further investigations should include the determination of the scattering length a of ^{164}Dy, which can be accomplished by a comparison of experimentally measured and theoretically calculated in-trap radii and stability diagrams. Our results should therefore stimulate experimental efforts to study dipolar BECs.

IV. ACKNOWLEDGEMENTS

We thank Holger Kadau, Thomas Maier, Matthias Schmitt and Tilman Pfau for valuable discussions.

[1] S. Ronen, D. C. E. Bortolotti, and J. L. Bohn, Phys. Rev. Lett. **98**, 030406 (2007).

[2] P. Köberle and G. Wunner, Phys. Rev. A **80**, 063601 (2009).

[3] I. Tikhonenkov, B. A. Malomed, and A. Vardi, Phys. Rev. Lett. **100**, 090406 (2008).

[4] P. Pedri and L. Santos, Phys. Rev. Lett. **95**, 200404 (2005).

[5] P. Köberle, D. Zajec, G. Wunner, and B. A. Malomed, Phys. Rev. A **85**, 023630 (2012).

[6] R. Eichler, D. Zajec, P. Köberle, J. Main, and G. Wunner, Phys. Rev. A **86**, 053611 (2012).

[7] L. Santos, G. V. Shlyapnikov, and M. Lewenstein, Phys. Rev. Lett. **90**, 250403 (2003).

[8] A. Griesmaier, J. Werner, S. Hensler, J. Stuhler, and T. Pfau, Phys. Rev. Lett. **94**, 160401 (2005).

[9] Q. Beaufils, R. Chicireanu, T. Zanon, B. Laburthe-Tolra, E. Maréchal, L. Vernac, J.-C. Keller, and O. Gorceix, Phys. Rev. A **77**, 061601 (2008).

[10] T. Lahaye, C. Menotti, L. Santos, M. Lewenstein, and T. Pfau, Rep. Progr. Phys. **72**, 126401 (2009).

[11] M. Lu, S. H. Youn, and B. L. Lev, Phys. Rev. Lett. **104**, 063001 (2010).

[12] M. Lu, N. Q. Burdick, S. H. Youn, and B. L. Lev, Phys. Rev. Lett. **107**, 190401 (2011).

[13] K. Aikawa, A. Frisch, M. Mark, S. Baier, A. Rietzler, R. Grimm, and F. Ferlaino, Phys. Rev. Lett. **108**, 210401 (2012).

[14] K.-K. Ni, S. Ospelkaus, M. H. G. de Miranda, A. Pe'er, B. Neyenhuis, J. J. Zirbel, S. Kotochigova, P. S. Julienne, D. S. Jin, and J. Ye, Science **332**, 231 (2008).

[15] T. Lahaye, J. Metz, B. Fröhlich, T. Koch, M. Meister, A. Griesmaier, T. Pfau, H. Saito, Y. Kawaguchi, and M. Ueda, Phys. Rev. Lett. **101**, 080401 (2008).

[16] T. Lahaye, T. Koch, B. Frohlich, M. Fattori, J. Metz, A. Griesmaier, S. Giovanazzi, and T. Pfau, Nature **448**, 672 (2007).

[17] M. A. Baranov, M. Dalmonte, G. Pupillo, and P. Zoller, Chemical Reviews **112**, 5012 (2012).

[18] C. Chin, R. Grimm, P. Julienne, and E. Tiesinga, Rev. Mod. Phys. **82**, 1225 (2010).

[19] Inouye S., Andrews M. R., Stenger J., Miesner H.-J., Stamper-Kurn D. M., and Ketterle W., Nature **392**, 151 (1998), 10.1038/32354.

[20] M. Abad, M. Guilleumas, R. Mayol, M. Pi, and D. M. Jezek, EPL **94**, 10004 (2011).

[21] S. Raghavan, A. Smerzi, S. Fantoni, and S. R. Shenoy, Phys. Rev. A **59**, 620 (1999).

[22] M. Abad, M. Guilleumas, R. Mayol, M. Pi, and D. M. Jezek, Phys. Rev. A **84**, 035601 (2011).